Direct growth of ZnO nanowire networks by catalyst-free chemical vapor deposition for ultraviolet-detecting application

Jiang Haitao[1,2], Liu Shibin[1], Yuan Qianqian[2]

(1. School of Electronics and Information, Northwestern Polytechnical University, Xi′an 710129, China;
2. Jiaozuo Teachers College, Jiaozuo 454001, China)

Abstract: High performance ultraviolet (UV) photodetectors (PDs) are critical for the high-speed optical communication and environmental sensing. Here, the performance of ZnO PDs was improved by directly fabricating photoelectric device on the ZnO nanowires(NWs) networks made by chemical vapor deposition (CVD) without any seed layer or metal catalyst. Results showed that the photocurrent of the ZnO NWs networks PDs is 60 μA, which was about 15 times of the single ZnO NW PDs. The response mechanism of ZnO NWs networks PDs was investigated in detail. Specially, the interconnections in ZnO NWs networks creat NW-NW junction barriers, which dominate the inter-wire charge transport. The fast tuning of NWs networks junction barrier height under the UV radiation, which contributes to the enhanced performance of the ZnO NWs networks UV PDs.

Key words: ultraviolet photodetector; ZnO nanowires networks; CVD; catalyst-free

CLC number: TN304.9; O472+4 **Document code:** A **DOI:** 10.3788/IRLA201847.1121002

无催化剂气相沉积法直接制备用于紫外光检测的氧化锌纳米线网

蒋海涛[1,2],刘诗斌[1],元倩倩[2]

(1. 西北工业大学 电子信息学院,陕西 西安 710129; 2. 焦作师范高等专科学校,河南 焦作 454001)

摘 要: 对于环境检测和高速光通信而言,高性能紫外光电探测器是关键。利用气相沉积法在无催化剂条件下制备氧化锌纳米线网,在纳米线网上直接制备光电器件的性能得到了提高。结果显示,纳米线网光电探测器的光电流为 60 μA,大约是单根纳米线光电器件光电流的 15 倍。详细讨论纳米线网光电探测器的响应机制发现,在纳米线网内,纳米线与纳米线之间的结势垒高度决定了纳米线内部载流子的传输。当紫外光照射纳米线网光电探测器时,纳米线与纳米线之间结势磊高度的快速变低,从而提高光电器件的性能。

关键词: 紫外光电探测器; 氧化锌纳米线网; 化学气相沉积法; 无催化剂

收稿日期:2018-06-10; **修订日期**:2018-07-12

基金项目:国家自然科学基金(61605207);河南省科技攻关项目(182102210419)

作者简介:蒋海涛(1978-),男,副教授,博士生,主要从事纳米材料的紫外光电探测器方面的研究。Email:jzchaonan@163.com

导师简介(通讯作者):刘诗斌(1960-),男,教授,博士,主要从事智能传感器系统和微电子器件与微传感器方面的研究。Email:liushibin@nwpu.edu.cn

0 Introduction

Benefitting from the large surface-to-volume ratio and the Debye length comparable to their small size, 1D semiconductor nanostructures are considered as the most promising building blocks for photodetectors with superior sensitivity, high quantum efficiency, and fast response speed [1]. The interest in developing high performance photodetectors has culminated in recent years in the realization of individual 1D semiconductor nanostructures fabricated by a top-down approach[2-7].

Among the semiconductor compounds, ZnO, especially, ZnO NWs, bearing large specific surface area, a direct and wide bandgap (~3.37 eV), size-dependent physical properties[8], fast charge transport characteristics[9], and high optical absorption in the UV range, are promising candidates for nanoelectronics and nanophotonics [10-12]. In the last two decades, ZnO NWs have been extensively exploited for sensing or detecting various of different physical phenomena such as typical nanoelectronic devices[13-15], various kinds of sensors [16-19], dilute magnetic semiconductor [20] and UV PDs[21,22]. To fully fulfill the potential in UV photodetection, a facile and safe achievement of the growth of ZnO NWs on SiO_2/Si substrate and an easy integration of ZnO NWs into UV PDs is still a challenge due to the limited capability of existing ZnO NWs preparation methods.

In this paper, we report the growth of lateral ZnO NWs networks by CVD without catalyst and comarpared the photoresponse behaviors of UV PDs based on the ZnO NWs networks and the single ZnO NWs, and discovered that the improvement photocurrent of the UV PDs based on the ZnO NWs networks. The mechanism of the enhanced performance was attributed to the UV tunable height of NW-NW junction barriers and the multi-channel junction structures in the ZnO NWs networks.

1 Experimental section

1.1 Pretreating of the substrate

The SiO_2/Si wafer was cleaned with acetone, ethanol and deionized water in turn with the help of ultrasound, and then the wafer was dried with a compressed nitrogen. Then, the substrate is heated for 1 min at 100 ℃ being coated with AZ3100 photoresist in a spin coater at 5 000 rpm. Then, the periodical square pillar microstructure with a top area size of 10 mm×10 mm and a height of around 800 nm was fabricated on substrate surfaces by Magnetic Enhanced Reactive Ion Etching (MERIE, SF6:CHF3 =15:40) after the UV lithography process.

1.2 Fabrication of ZnO NWs networks and characterization

The mixture of the ZnO powder (99.99%) and nanodiamond powder (weight ratio 3:1) were used as the precursor and loaded in an alumina boat located at the center of an alumina tube (100 cm), which was placed in a single-zone horizontal tube furnace serving as the reaction chamber. The treated SiO_2 side with the periodical square pillar microstructure facing the source. Argon gas was used as the carrier gas at a flow rate of 100 standard cubic centimeters per minute (sccm) throughout the experiment to transport the ZnO vapors downstream for the ZnO NWs growth. When the temperature was heated to 600 ℃, the high purity O_2 gas was introduced into the quartz tube at the rate of 2 sccm. The furnace was heated to 960 ℃ and held at this temperature for 30 minutes under the pressure of 30 kPa. Then the tube was cooled down to room temperature under an argon gas flow.

The morphology and crystal structure of ZnO NWs networks were characterized by high-resolution transmission electron microscopy (TEM, JEM2100), field emission scanning electron microscope (SEM, JEOL7600) and X-ray diffractometer (XRD) (Rigaku RINT2500 TRAX-III, Cukα radiation).

1.3 Device fabrication and characterization

To fabricate the ZnO NWs networks PDs, the silver paint was directly applied onto the as-prepared ZnO NWs to form the electrodes with internal space around 4 mm and enough thickness. The fabrication of

the single NW-based devices with traditional lithographic process is very challenging. The as-prepared ZnO NWs were first dispersed into alcohol with the help of ultrasound. To avoid forming of ZnO NWs networks, the concentration of ZnO NWs suspension should be very low. A droplet of the ZnO NWs suspension was dropped over the interdigital microelectrodes (with digital spacing of 10 μm), and then dried at 140 ℃ for 30 mins to vaporize the solvent.

Photoresponse testing was performed on the Semiconductor Characterization System (keithly 4200-SCS). The sampling period was set to 20 s, and the change in current of the UV photodetector with or without light illumination was recorded by the Semiconductor Characterization System. A portable UV light source was adopted, and the UV power density incident to the device surface is estimated to be 1.35 mW/cm $^{-2}$. The "on" and "off" of the illumination were controlled by a chopper. All of the above measurements were conducted in a darkroom to minimize the influence of natural light.

2 Results and discussion

2.1 ZnO NWs networks characterization

SEM was used to characterize the morphology of the products. Figure 1 (a) exhibits the top view SEM images of the synthesized ZnO NWs networks with souce materials as mentioned in the experimental section, and Fig.1(b) shows the high resolution of the crossponding samples. From Fig.1 (b), we found that the multi-channel junctions formed between ZnO NWs. Fig.1(c) displays the high-resolution TEM image of one single ZnO nanowire used for TEM. Fig.1(d) reveals the spacing of 2.6 Å (1 Å=10^{-10} m) between adjacent fringes corresponds to the distance between two (002) crystal planes the inset selected area electron diffraction (SAED) image also confirms the single crystallinity and growth direction of [001] for the ZnO NWs.

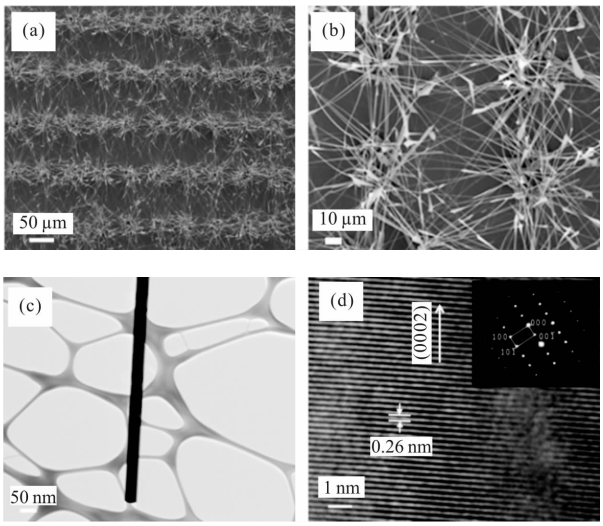

Fig.1 Characterizations on ZnO NWs networks synthesised via CVD((a) top view SEM images of the as-grown ZnO NWs networks; (b) high resolution of the ZnO NWs networks; (c) the sample of the ZnO NWs used for TEM; (d) TEM images of single ZnO NWs with the adjacent fringe distance of 0.26 nm and the growth direction of [001], the insert image is the SAED pattern of the ZnO NWs indicating single crystallinity of ZnO NWs)

2.2 Photoresponse of ZnO NWs device

The current-voltage (I-V) measurements of the device were carried out at ambient condition with UV illumination (365 nm, 1.35 mW/cm^2). And the photoresponse of the "on" and "off" to UV illumination were controlled by a metal chopper. The photoresponse behaviors of both ZnO NWs networks-based and single ZnO NW-based PDs under UV light illumination with the bias voltage of 2 V are shown in Fig.2. Figure 2 (a) shows $I-V$ curves of the ZnO NWs networks photodetector and with and without light illumination. The asymmetrical $I-V$ transport curve indicated Schottky contacts between Au and ZnO NWs. Before UV light was applied, the measured current was observed to be very low. The dark current (I_{dark}) is around 10 μA. However, after exposure of the device to UV light, the photocurrent (I_{light}) jumps to around 61 μA, as shown in Fig.2(b). It is obvious that a significant increase in the source

drain current was observed upon exposing the device to UV radiation, which implied a pronounced increase in conductance. Figure 2 (c) shows $I-V$ curves of single ZnO NW-based PD with and without light illumination. The I_{dark} of single NW device is around 10 nA; while the current could drastically increase to 4.1 μA once the UV illumination is on, as shown in Fig.2(d).

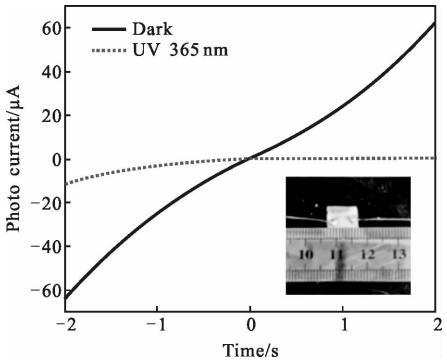

(a) $I-V$ transport curves of ZnO NWs networks PD with UV illumination "on" and "off"

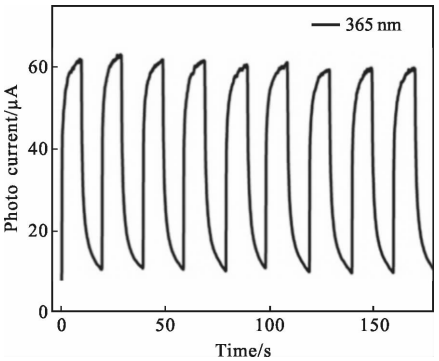

(b) Time-resolved photocurrent rise and decay of ZnO NWs networks PD with UV illumination "on" and "off" periods of 20 s

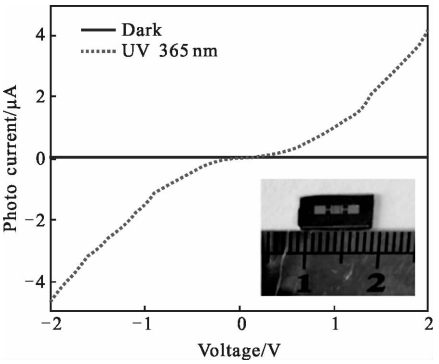

(c) $I-V$ transport curves of single ZnO NWs PD with UV illumination "on" and "off"

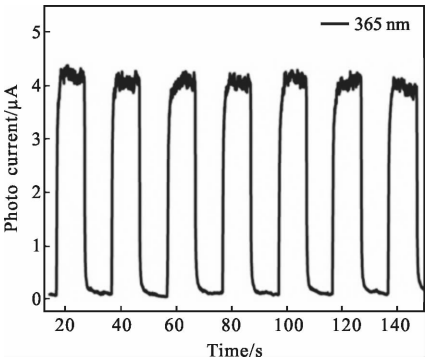

(d) Time-resolved photocurrent rise and decay of single ZnO NW PD with UV illumination "on" and "off" periods of 20 s

Fig.2 Photoresponse behaviors of ZnO NWs nerworks PD and single NW PD under UV light illumination with both "on" and "off" periods of 20 s(The bias voltage applied to the devices is 2 V)

The response time is an important indicator of merit of photodetector. The time-dependent photocurrent at 2 V bias with multiple UV on/off cycles was measured, in which both the "on" and "off" time of the UV illumination are 10 s. To estimate the rise and decay time constants, one cycle of UV illumination under a power density of 1.35 mW/cm^2 was fitted using bi-exponential [23] expression of the form

$$I=I_0+A\mathrm{e}^{(t/t_{on})}$$
$$I=I_0+B\mathrm{e}^{(t/t_{off1})}+C\mathrm{e}^{(t/t_{off2})} \quad (1)$$

where t_{on}, t_{off1} and t_{off2} represent the relaxation time constants, whereas I_0, A, B and C are positive constants.

Figure 3 (a) and (b) show typical time-resolved photocurrent rise and decay stages of ZnO NWs networks device, with and without UV illumination, respectively. By fitting the photocurrent data versus the time using the Eq. (1), we estimated the time constants of the rising relaxation time ton was about 0.609 s, whereas the decaying relaxation times were estimated as follows: t_{off1}=0.287 s and t_{off2}=2.509 s, with relative weight factors of 58.9 and 41.1%, respectively, and the average decay time constant t_d is calculated to be 1.20 s. Figure 3 (c) and 3 (d) give time-resolved photocurrent variation curves of single ZnO NW

device, with and without UV illumination, respectively. By fitting the photocurrent data versus the time using the Eq. (1), we estimated the time constants of the rising relaxation time ton was about 0.293 s, whereas the decaying relaxation times were estimated as follows: t_{off1}=0.24 s and t_{off2}=0.87 s, with relative weight factors of 99.9% and 0.1%, respectively, and the average decay time constant td is calculated to be 0.24 s. It was found that the single NW device is faster than the NWs networks PD both the rise process and the decay process. The slightly longer rise time of ZnO NWs networks device could mainly be attributed to the much longer channel of the ZnO NWs networks PD ($L\approx$4 mm for ZnO NWs networks device which $L\approx$10 μm for single NW device).

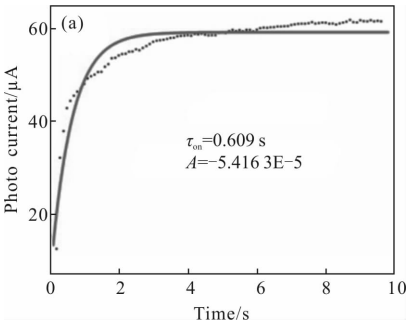

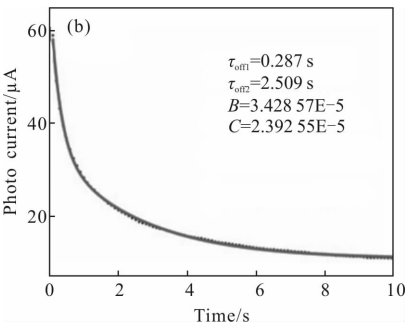

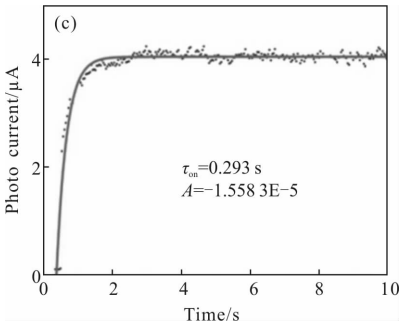

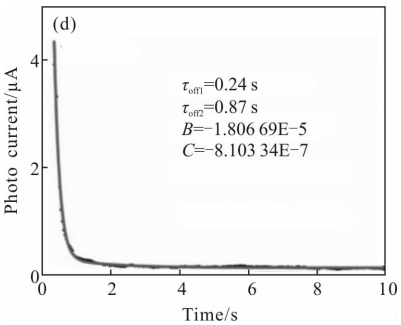

Fig.3 Photoresponse speed of different ZnO NW-based UV PDs ((a) and (b) are typical rise and decay curves for ZnO NW networks PD under UV illumination of "on" and "off" with period of 20 s; (c) and (d) are typical rise and decay curve of single ZnO NW PD under UV illumination of "on" and "off" with period of 20 s)

2.3 Discussion

It is well accepted that the chemisorption/desportion of oxygen molecules governs photogeneration of free carriers in ZnO: (1) the oxygen molecules absorbed on the surface of ZnO NWs to form O_2 by capturing free electrons from ZnO NW surface, creating a highly resistive depletion layer near the ZnO NWs surface; (2) Under UV illumination, electron-hole pairs are generated, the holes migrate to the surface and combine with adsorbed oxygen molecules O_2^-, resulting in desorption of oxygen from the ZnO surface (as illustrated in Fig.4(a)). This hole-trapping process leads to an increase in the free-carrier concentration and a decrease in the width of the depletion layer, producing an apparent enhancement in photocurrent. When the UV irradiation is switched off, holes recombine with electrons, and oxygen molecules are readsorbed on the ZnO NW surface by capturing electrons, which increases the resistance of the device again. Thus, decrease in diameter of ZnO NW could increase the relative width of the depletion layer and thus enhance the photo-to-dark current ratio.

The photoconductive mechanism of the ZnO NWs networks PDs includes the photogeneration of free carriers and the carriers transport across the interface between two neighboring NWs and the metal/ZnO interface. Both the single ZnO NW PDs

and the ZnO NWs networks PDs have the same mechanism of photogeneration free carriers and interface between Ag and ZnO. Here, the focus is on the carriers transport between two neighboring NWs. In the ZnO NWs networks PD, apart from the oxygen chemisorption/desorption-related process, a NW−NW junction barrier is generated between interconnected ZnO NWs, which are not readily available in single NW−based devices. The network can be regarded as a percolated network of ZnO NWs, whose junction resistance is usually several orders of magnitude larger than that of an individual ZnO NW[24]. It is reported that the electron conduction in percolated NW networks is dominated by the NW−NW junction barriers, electrons must overcome the junction barrier to transport from one NW to another[24-25]. The junction barrier height caused by the SBB effect could be estimated by[26-27]:

$$\varphi_{jb} \propto eN_d t_c^2 / \varepsilon_r \varepsilon_0$$

where e is elemental charge; N_d is space charge density caused by the oxygen chemisorption; t_c is the thickness of depletion area and ε0εr is the dielectric constant of ZnO. The tunnelling current across the junction barrier is in an exponential relation to the barrier height:

$$I \propto \exp(-\varphi_{jb}/kT)$$

where k is the Boltzmann constant and T is temperature. Hence, the current is very sensitive to small changes in the barrier height.

Under UV excitation, the space charge density N_d, and the thickness of depletion area t_c would be greatly decreased, and thus the junction barriers would be low enough for charge transport. The improvement in the rise time of the ZnO NWs network PD can be attributed to the NW−NW junction barrier controlled charge transport, as shown in Fig.4(b). Since the photo-desorption of oxygen from the NW channel is a relatively slow process[28], thus the response speed will be relatively slow, if the device conductance is controlled by the NW conductance only, such as the single NW device, as displayed in Fig.4(a). Once the UV illumination is off, the barrier height would increase significantly, as a result of electron-hole recombination. The dominant effect of the junction barrier leads to a fast current decay, because the photo induced barrier height modulation is typically much faster than the oxygen diffusion process. Though we also observed that the photocurrent decay time of ZnO NWs network UV PD is slightly longer than that of the smaller single ZnO NW device, we tentatively ascribed it to the large size of ZnO NWs network PD.

Anoter findings is the multi-channel junction structures in the ZnO NW network. As shown in Fig.1(b), there exist a large amount of such multi-channel junction structures in the ZnO NW network. As schematically displayed in Fig.4, these structures have lager specific surface area than single nanowire and thus more oxygen adsorbed at the surface. In addition, the large specific area can receive more UV light when the light is on, and thus a larger photocurrent could be obtained in ZnO NWs network device compared with that of single ZnO device.

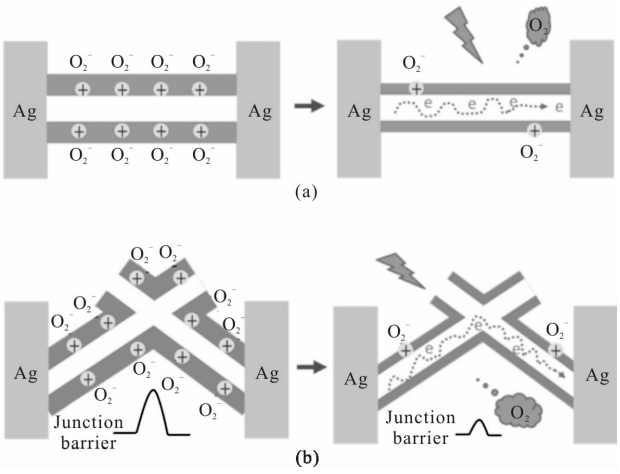

Fig.4 Schematic illustration the working mechanism of ZnO NWs networks device and single ZnO NWs device. (a) Carrier generation in a single ZnO NWs PD; (b) Carrier generation and transport in ZnO NWs networks PDs. The UV excitation generates electron-hole pairs, the holes will transport to the ZnO surface and neutralize the adsorbed O_2^- the unpaired electrons decrease the thickness of depletion area and enhance the conductivity of ZnO NW

3 Conclusion

In summary, we found that the responses peed of ZnO NWs UV PDs could be improved by directly fabricating UV PDs on entangled ZnO NW arrays grown on SiO_2 through a catalyst-free CVD process. The mechanism of the enhancement in response speed was attributed to the UV tunable height of NW-NW junction barriers, because the photo-induced barrier height modulation is typically much faster than the oxygen chemisorption/desorption process. We believe the strategy shown here would greatly prompt the application of ZnO nanostructures in nanoelectronics and optoelectronics.

References:

[1] Ramgir N S, Yang Y, Zacharias M. Nanowire-based sensors [J]. ***Small***, 2010, 6(16): 1705-1722.

[2] Zhang L, Fang M. Nanomaterials in pollution trace detection and environmental improvement [J]. ***Nano Today***, 2010, 5 (2): 128-142.

[3] Fang X, Zhai T, Gautam U K, et al. ZnS nanoparticles: from synthesis to applications [J]. ***Progress in Materials Science***, 2011, 56(2): 175-287.

[4] Konstantatos G, Sargent E H. Nanostructured materials for photon detection [J]. ***Nature Nanotechnology***, 2010, 5 (6): 391-400.

[5] Xia F, Mueller T, Lin Y M, et al. Ultrafast graphene photodetector[J]. ***Nature Nanotechnology***, 2009, 4(12): 839-843.

[6] Taniyasu Y, Kasu M, Makimoto T. An aluminium nitride light-emitting diode with a wavelength of 210 nanometres [J]. ***Nature***, 2006, 441(7091): 325-328.

[7] Yang Zhi, Wang Minqiang, Zhang Miao, et al. All-inorganic perovskite nanocrystal film photodetector. [J] ***Infrared and Laser Engineering***, 2018, 47(9): 0920007. (in Chinese)

[8] Yang P, Yan H, Mao S, et al. Controlled growth of ZnO nanowires and their optical properties [J]. ***Advanced Functional Materials***, 2002, 12(5): 323-331.

[9] Law M, Greene L E, Johnson J C, et al. Nanowire dye-sensitized solar cells[J]. ***Nature Materials***, 2005, 4(6): 455-459.

[10] Retamal J R D, Chen C Y, Lien D H, et al. Concurrent improvement in photogain and speed of a metal oxide nanowire photodetector through enhancing surface band bending via incorporating a nanoscale heterojunction [J]. ***Acs Photonics***, 2014, 1(4): 354-359.

[11] Liu X, Gu L, Zhang Q, et al. All-printable band-edge modulated ZnO nanowire photodetectors with ultra-high detectivity[J]. ***Nature Communications***, 2014, 5(4007): 1-9.

[12] Nasiri N, Bo R, Chen H, et al. Structural engineering of nano-grain boundaries for low-voltage UV-photodetectors with gigantic photo-to dark-current ratios [J]. ***Advanced Optical Materials***, 2016, 4(11): 1787-1795.

[13] Ju S, Facchetti A, Xuan Y, et al. Fabrication of fully transparent nanowire transistors for transparent and flexible electronics[J]. ***Nature Nanotechnology***, 2007, 2(6): 378.

[14] Huang H, Liang B, Liu Z, et al. Metal oxide nanowire transistors[J]. ***Journal of Materials Chemistry***, 2012, 22(27): 13428-13445.

[15] Hou T N, Han J, Yamada T, et al. Single crystal nanowire vertical surround-gate field-effect transistor[J]. ***Nano Letters***, 2004, 4(7): 1247-1252.

[16] Xue F, Zhang L, Tang W, et al. Piezotronic effect on ZnO nanowire film based temperature sensor [J]. ***ACS Applied Materials & Interfaces***, 2014, 6(8): 5955-5961.

[17] Jiang C, Song J. Significant photoelectric property change caused by additional nano-confinement: A study of half-dimensional nanomaterials[J]. ***Small***, 2014, 10(24): 5042-5046.

[18] Wang X, Summers C J, Wang Z L. Large-scale hexagonal-patterned growth of aligned ZnO nanorods for nano-optoelectronics and nanosensor arrays [J]. ***Nano Letters***, 2004, 4(3): 423-426.

[19] Fulati A, Ali S M U, Riaz M, et al. Miniaturized pH sensors based on zinc oxide nanotubes/nanorods[J]. ***Sensors***, 2009, 9(11): 8911-23.

[20] Wang D D, Xing G Z, Yan F, et al. Ferromagnetic (Mn, N)-codoped ZnO nanopillars array: experimental and computational insights[J]. ***Applied Physics Letters***, 2014, 104 (2): 1.

[21] Kurtis S Leschkies, Ramachandran Divakar, Joysurya Basu, et al. Photosensitization of ZnO nanowires with CdSe quantum dots for photovoltaic devices [J]. ***Nano Letters***, 2007, 7(6): 1793-1798.

[22] Zhan Z, Zheng L, Pan Y, et al. Self-powered, visible-light photodetector based on thermally reduced graphene oxide-

ZnO (rGO-ZnO) hybrid nanostructure [J]. ***Journal of Materials Chemistry***, 2012, 22(6): 2589-2595.

[23] Guo L, Zhang H, Zhao D, et al. High responsivity ZnO nanowires based UV detector fabricated by the dielectrophoresis method [J]. ***Sensors & Actuators B Chemical***, 2012, 166-167(10): 12-16.

[24] Chen M, Hu L, Xu J, et al. ZnO hollow-sphere nanofilm-based high-performance and low-cost photodetector [J]. ***Small***, 2011, 7(17): 2449-2453.

[25] Peng S M, Su Y K, Ji L W, et al. ZnO nanobridge array UV photodetectors [J]. ***Journal of Physical Chemistry C***, 2010, 114(7): 3204-3208.

[26] Calarco R, Marso M, Richter T, et al. Size-dependent photoconductivity in MBE-grown GaN-nanowires [J]. ***Nano Letters***, 2005, 5(5): 981-984.

[27] Sysoev V V, Button B K, Wepsiec K, et al. Toward the nanoscopic "electronic nose": hydrogen vs carbon monoxide discrimination with an array of individual metal oxide nano- and mesowire sensors [J]. ***Nano Letters***, 2006, 6(8): 1584-1588.

[28] Nasiri N, Bo R, Fu L, et al. Three-dimensional nano-heterojunction networks: a highly performing structure for fast visible-blind UV photodetectors [J]. ***Nanoscale***, 2017, 9(5): 2059-2067.